Vehicle Design and Optimization Model for Urban Air Mobility

Arthur Brown* and Wesley L. Harris†
Massachusetts Institute of Technology, Cambridge, Massachusetts 02139

https://doi.org/10.2514/1.C035756

Urban air mobility refers to an envisaged air taxi service, using small, autonomous, vertical-takeoff-and-landing, battery-powered electric aircraft. A conceptual design and optimization tool for urban air mobility, including vehicle, mission, and cost models, is presented in this paper. The tool uses geometric programming, a class of optimization problems with extremely fast solve times and for which global optimality is guaranteed. The tool is used to conduct a study of urban air mobility from a vehicle design perspective. Vehicle configurations with a higher lift-to-drag ratio, but a higher disk loading, generally weigh less and cost less to operate. The battery and the pilot are identified as the two main cost drivers; strategies for reducing these two costs are discussed. A case study is conducted on New York City airport transfers; trip times and costs are compared with those of current helicopter air taxi operations and with car ride-sharing. Sensitivity analyses are presented with respect to reserve requirements, mission range, and battery energy density. A battery energy density of 400 Wh/kg is shown to be a critical enabling value for urban air mobility.

Nomenclature

A	=	rotor disk area; πR^2, m^2
A_b	=	rotor blade area; $B\bar{c}R$, m^2
AR	=	aircraft wing aspect ratio, b^2/S
a_j	=	jth exponent
B	=	number of rotor blades
b	=	aircraft wingspan, m
C_{D_0}	=	aircraft three-dimensional zero-lift drag coefficient
C_{d_0}	=	rotor blade two-dimensional zero-lift drag coefficient
C_L	=	aircraft wing three-dimensional lift coefficient
$\overline{C_l}$	=	rotor mean lift coefficient, $3C_T/s$
C_P	=	rotor power coefficient, $P/(0.5\rho V_T^3 A)$
C_{P_i}	=	rotor ideal power coefficient, $0.5C_T^{3/2}$
C_{P_p}	=	rotor profile power coefficient, $0.25sC_{d_0}$
C_T	=	rotor thrust coefficient, $T/(0.5\rho V_T^2 A)$
c	=	monomial leading coefficient
$\bar{c}$	=	average rotor blade chord, m
dr	=	deadhead ratio
E_b	=	battery electrical energy, kWh
e	=	wing span efficiency
FOM	=	rotor figure of merit, $C_{P_i}/(k_i C_{P_i} + C_{P_p})$
f_e	=	empty mass fraction
k	=	aircraft induced power factor, $1/(\pi eAR)$
k_i	=	rotor induced power factor
L/D	=	vehicle lift-to-drag ratio
M_{tip}	=	rotor tip Mach number
$m(\boldsymbol{x})$	=	monomial function of $\boldsymbol{x}$
N	=	number of rotors
n_m	=	number of monomial equality constraints
n_p	=	number of posynomial inequality constraints
P	=	shaft power, kW
$p(\boldsymbol{x})$	=	posynomial function of $\boldsymbol{x}$
R	=	rotor radius, m
S	=	wing reference area, m^2
s	=	rotor solidity, A_b/A
T	=	thrust generated by one rotor, N
T/A	=	rotor disk loading, N/m^2
t_{boarding}	=	boarding time (time required to load/unload an air taxi, conduct safety checks, etc.)
t_{flight}	=	flight time
t_{ground}	=	ground time (time required to travel to a heliport)
$t_{\text{rideshare}}$	=	time required for a car ride-sharing trip
V	=	airspeed, m/s
W	=	weight, N
$\boldsymbol{x}$	=	vector of design variables x_j
x_j	=	jth design variable
η	=	system efficiency
ρ	=	air density, kg/m^3

I. Introduction

URBAN air mobility (UAM), also known as on-demand aviation (ODA), is an envisaged air taxi service. The service would use electric vertical takeoff and landing (eVTOL) aircraft[‡] with 1–4 seats for trips of approximately 370 km (200 nmi) or less [1]. In general, multiple electric motors and propellers are used; this design strategy is known as distributed electric propulsion (DEP). DEP is enabled because electric motors, unlike internal-combustion engines, are efficient at a wide range of sizes.

In theory, UAM offers a number of advantages over existing transport solutions. Firstly, commute times can be reduced and/or mobility reach increased[§] relative to cars, because eVTOL vehicles can avoid gridlock and overfly obstacles. Secondly, costs can be reduced. Electric motors have fewer moving parts and operate at lower temperatures relative to combustion engines, resulting in lower maintenance costs; eVTOL vehicles use electricity instead of fuel, resulting in reduced energy costs relative to fuel-burning cars and helicopters [2]; and eVTOL vehicles can be autonomous, resulting in cost savings relative to modes of transportation with a driver or pilot. Thirdly, environmental impact can be reduced, also due to the use of electric propulsion. For example, eVTOL vehicles may produce less community noise relative to helicopters; they emit no greenhouse gases that contribute to climate change; and (unlike general-aviation aircraft with piston engines) they produce no lead emissions.

This research examines UAM from the perspective of an eVTOL vehicle designer. The goals are to determine whether eVTOL vehicles are technically feasible; to gain estimates for key vehicle design parameters such as mass and cost; and to compare costs with other transportation options.

Dozens of companies are developing eVTOL vehicles, including Joby Aviation, Lilium Aviation, A^3 by Airbus, and Aurora Flight Sciences. A variety of vehicle configurations are employed.

Presented as Paper 2018-0105 at the AIAA SciTech Forum, Kissimmee, FL, January 8–12, 2018; received 3 October 2019; revision received 18 February 2020; accepted for publication 30 July 2020; published online Open Access 29 October 2020.

*Ph.D. Candidate, Department of Aeronautics and Astronautics, 77 Massachusetts Avenue. Student Member AIAA.

†Charles Stark Draper Professor, Department of Aeronautics and Astronautics, 77 Massachusetts Avenue. Fellow AIAA.

‡Most proposed aircraft concepts are fully electric, although some are hybrid electric.

§Mobility reach is the accessible land area with a given commute time [1].

Table 1 Design variables and inputs

		Constant input	
Model	Design variable	Universal	Configuration specific
Aircraft model	Max takeoff mass	Battery energy density	Empty mass fraction
	Battery mass	Battery power density	Number of rotors
	Rotor diameter	Usable battery energy fraction	Cruising speed
		Electrical efficiency	Cruise lift-to-drag ratio
		Propulsive efficiency	Max hover disk loading
		Number of rotor blades	Rotor max mean lift coefficient
		Rotor-induced power factor	Tail-rotor power fractions
		Rotor zero-lift drag coefficient	
		Rotor solidity	
		Rotor max tip Mach number	
		Air density	
		Speed of sound	
Mission model	Rotor tip speeds	Table 4	— —
Cost model	— —	Table 5	— —

For example, Joby Aviation's S4 is a tilt-rotor design; Lilium Aviation uses a tilt-duct design; Airbus's Vahana is a tilt-wing; and Aurora Flight Sciences uses a lift + cruise design (a design with separate rotors for cruise and for hover, with no folding or tilting components). Other postulated configurations include the multirotor, the autogyro, the conventional helicopter, the tilt duct, the coaxial-rotor helicopter, and the compound helicopter [3]. This research also aims to provide guidance to vehicle designers on the strengths and weaknesses of each configuration.

The rest of this paper is structured as follows. The methodology, including the optimization algorithm, vehicle model, mission model, and cost model, is given in Sec. II. A trade study between eVTOL configurations, a case study on New York City airport transfers, and three sensitivity analyses are presented in Sec. III. Finally, conclusions are given in Sec. IV.

II. Methodology

The optimization tool developed in this work uses cost per trip as the objective function. Vehicle and mission models are similar to those from McDonald and German [3]. Some input parameters, such as battery energy density and usable energy fraction, are universal (i.e., held constant between vehicle configurations). Other input parameters, such as empty mass fraction, cruising speed, cruise lift-to-drag ratio, and maximum hover disk loading, are varied between configurations, using representative values for a given configuration.

However, in this study, optimization is used instead of sizing. Instead of fixing the vehicle mass and empty mass fraction and then computing the range, the tool fixes the empty mass fraction and mission range and then computes the vehicle mass during the optimization process. This means that all configurations have the same range, enabling comparisons between them.

Design variables and inputs are summarized in Table 1.

A. Geometric Programming

The optimization tool is formulated as a geometric program (GP), a type of constrained optimization problem. A GP can be written as follows [4]:

$$\begin{aligned} \text{Minimize} \quad & p_0(\boldsymbol{x}) \\ \text{Subject to} \quad & p_i(\boldsymbol{x}) \leq 1, i = 1, \ldots, n_p \\ & m_i(\boldsymbol{x}) = 1, i = 1, \ldots, n_m \end{aligned} \tag{1}$$

$p_0(\boldsymbol{x})$ is the objective function (a posynomial function), subject to n_p posynomial inequality constraints $p_i(\boldsymbol{x})$ and n_m monomial equality constraints $m_i(\boldsymbol{x})$. The vector $\boldsymbol{x}$ represents the design variables. Monomial functions $m(\boldsymbol{x})$ and posynomial functions $p(\boldsymbol{x})$ are defined in Eqs. (2) and (3), respectively:

$$m(\boldsymbol{x}) = c \prod_{j=1}^{n} x_j^{a_j} \tag{2}$$

$$p(\boldsymbol{x}) = \sum_{i=1}^{K} c_i \prod_{j=1}^{n} x_j^{a_j} \tag{3}$$

c and x_j must be positive, whereas a_j can be any real number. A posynomial is simply a sum of monomial terms.

GPs cannot be applied to solve general nonlinear optimization problems, because of the limitations imposed by Eq. (1). In return, GPs offer extremely fast solve times, require no initial guesses, and guarantee a globally optimal solution if one exists [5]. GPs are increasingly being applied to optimization problems in aerospace, ranging from high-altitude, long-endurance (HALE) aircraft to electric short takeoff and landing (eSTOL) aircraft [6,7].

The GPs in this project were developed using the open-source Python package GPkit,[¶] with MOSEK as the numerical solver. A typical optimization run takes approximately 0.05 s to converge on a laptop computer running Windows 10 with an Intel Core i7 processor.

B. Vehicle Model

1. Components

The vehicle model is divided into four components: airframe, battery, electrical system, and rotors. The airframe model uses a constant empty mass fraction f_e, relative to the maximum takeoff mass. Meanwhile, the battery model uses a pack-level energy density and power density and sizes the battery accordingly. Only 80% of the battery energy is usable (including reserves), to prevent current spikes at low charge levels and also to extend battery life. The airframe and battery have their own mass models; the mass of the other two components is bookkept under airframe mass.

The electrical system applies a constant efficiency to the power coming from the batteries; it accounts for losses due to the wires, controller, and motors. Finally, the rotor model is used only in hover; it is described in Sec. II.B.3.

2. Cruise Performance

The range and endurance of an electric aircraft in cruise can be computed using Eqs. (4) and (5), respectively:

$$\text{Range} = \eta \frac{L}{D} \frac{E_b}{W} \tag{4}$$

$$\text{Endurance} = \eta \frac{L}{D} \frac{E_b}{VW} \tag{5}$$

[¶]GPkit can be downloaded from GitHub here: https://github.com/convexengineering/gpkit.

Table 2 Vehicle model input parameters

Parameter	Value
Battery energy density	400 Wh/kg
Battery power density	3 kW/kg
Usable battery energy fraction	80%
Electrical efficiency	90%
Propulsive efficiency	85%

Table 3 Rotor model input parameters

Parameter	Symbol	Value
Number of rotor blades	B	5
Induced power factor	k_i	1.2
Zero-lift drag coefficient	C_{d_0}	0.01
Rotor solidity	s	0.1
Maximum tip Mach number	$(M_{\text{tip}})_{\max}$	0.9

L/D is the vehicle lift-to-drag ratio, E_b is the battery energy used, W is the vehicle weight, and V is the airspeed. η is the system efficiency, equal to the product of electrical and propulsive efficiency. For a propeller-driven aircraft, propulsive efficiency is equal to propeller efficiency; a value of 85% is used.

Vehicle parameters are summarized in Table 2. Empty mass fraction, lift-to-drag ratio, and cruising speed are configuration-specific parameters and as such are discussed later (Sec. III.A.1).

3. Hover Performance

In hover, the rotors must produce thrust equal to vehicle weight. An extension of actuator-disk theory is used to predict rotor performance in hover, providing a connection between rotor thrust T and motor shaft power P. The model and coefficient conventions from Ref. [8] are used.

The optimizer treats rotor tip speed V_T as a design variable. The upper limit on tip speed is a limit on the tip Mach number, whereas a lower limit is set by limiting the blade mean lift coefficient $\overline{C_l}$. Standard sea-level values for air density and speed of sound are used.

Parameters used by the rotor model are given in Table 3. Maximum hover disk loading is a configuration-specific parameter and as such is discussed later (Sec. III.A.1).

C. Mission Model

The mission model includes three different mission profiles:

1) In a sizing mission, the aircraft must be capable of flying.

2) In a revenue mission, the aircraft is carrying paying passengers.

3) In a deadhead mission, the aircraft is relocated for its next revenue-generating flight.[**]

A diagram of the mission profiles is given in Fig. 1. Note that transition and climb segments are not included.

The sizing mission includes a longer hover time relative to the revenue and deadhead missions. It also includes a reserve, a 20-min loiter time, required by the FAA for helicopter visual flight rules (VFR) operations [9]. This requirement would be applicable if eVTOL vehicles are certified as helicopters.

The mission time for the revenue and deadhead missions includes time spent on the ground, which is constrained by one of two factors. The time has to be greater than 5 min, to allow for passenger loading/unloading, safety checks, etc. Meanwhile, the battery is charged simultaneously; all of the energy used during the mission is replenished. A 200 kW charger and a 90% charging efficiency are used for the purposes of computing charging time.[††]

Two crew options are available: piloted and autonomous. If the mission is piloted, the pilot adds 86 kg (190 lbs) to the vehicle mass.

**Deadhead missions do not generate revenue because no passengers are carried, but they must be accounted for during cost analysis.

††Current Tesla Superchargers can produce as much as 250 kW [10].

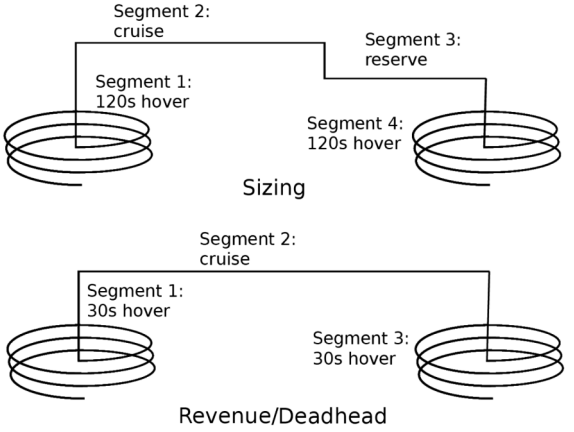

Fig. 1 Mission profiles.

If the mission is autonomous, no mass penalty is applied, and 91 kg (200 lbs) per passenger is assumed.

Mission inputs are summarized in Table 4.

Note from Table 4 that the deadhead mission is flown autonomously. This is done primarily to demonstrate the flexibility of the methodology. In practice, the deadhead mission cannot always be autonomous, as pilots will need to be relocated along with their aircraft in order to fly piloted revenue missions.

D. Cost Model

The cost model uses both the revenue mission and the deadhead mission. Costs are divided into capital expenses and operating expenses. Input parameters are given in Table 5.

1. Capital Expenses

Capital expenses are subdivided into three categories: airframe purchase price, battery purchase price, and avionics purchase price. Airframe purchase price is computed using a fixed price per unit

Table 4 Mission model input parameters

Mission	Sizing	Revenue	Deadhead
Piloted?	Yes	Yes	No
Pilot mass, kg	86	86	— —
Mission range, km	93	56	56
Passengers	3	2	0
Mass per passenger, kg	91	91	— —
Reserve, min	20	— —	— —
Hover time	2 min	30 s	30 s
Charger power, kW	— —	200	200
Charging efficiency, %	— —	90	90

Table 5 Cost model input parameters

Parameter	Value
Airframe purchase price	$1102 per kg
Airframe lifetime	10,000 hours
Avionics purchase price	$100,000
Avionics lifetime	10,000 hours
Battery purchase price	$400 per kWh
Battery lifetime	800 cycles
Pilot wrap rate	$100 per hour
Pilots per aircraft	1.5
Aircraft per bunker pilot	6
Maintenance man-hours	0.6 per flight hour
Mechanic wrap rate	$60 per hour
Price of electricity	$0.12 per kWh
Indirect operating cost	40% of DOC
Deadhead ratio	35%
Cost margin	10%

Table 6 Purchase price per unit empty mass for several representative aircraft

Vehicle	Category	Price per kg
Cessna 172S	Four-seat lightplane	$525
R44 Raven II	Four-seat helicopter	$696
525 Citation M2	Light business jet	$1536

airframe mass, whereas battery purchase price is computed using a fixed price per unit energy capacity.

Purchase price per unit empty mass data were obtained from Ref. [11], for several different aircraft categories. Results are in Table 6.

Table 6 shows that price per unit empty mass varies widely depending on the aircraft category. The Cessna 172 and Robinson R44 are relatively simple designs that have been in production for decades (since 1956 and 1992, respectively). Their cost per unit empty mass values are substantially lower than those of the Cessna Citation M2, a much more sophisticated aircraft that entered production in 2013 [11]. As a compromise, an estimate of $1102 per kg ($500 per lb) is used in this work. An additional $100,000 per vehicle is added, as an estimate for the cost of the additional avionics required for autonomous flight. Finally, a battery purchase price per unit energy capacity of $400 Wh/kg is based upon Department of Energy projections [12].

Capital expenses are amortized over the mission, using straight-line depreciation with no salvage value. Vehicle and avionics costs are amortized assuming that the vehicle is operated 2000 h per year for 5 years before retirement. This leads to a 10,000 h service life. For comparison, business aircraft are typically operated 500–2000 h per year [13].

It is more appropriate to amortize a battery using a cycle life instead of a lifetime measured in hours. Severson et al. [14] experimentally obtained the cycle lives of 124 commercially available lithium iron phosphate/graphite (a type of lithium-ion) battery cells, at C rates representative of fast-charging conditions. Cycle life was defined as the number of cycles until the battery reached 80% of its nominal capacity. Their obtained average cycle life of 806 cycles is close to the value of 800 cycles used in this work.

2. *Operating Expenses*

Operating expenses are divided into direct operating cost (DOC) and indirect operating cost (IOC). DOC is further subdivided into three categories: pilot cost, maintenance cost, and energy (electricity) cost.

Pilot costs are estimated using wrap rates. A wrap rate is a cost per unit mission time, including the time spent on the ground. Wrap rates include salary payments as well as benefits, overhead, training, administrative costs, etc. [13]. Wrap rates of $50–$150 per hour are typical for business aviation pilots [15]; the median value is used in this work.

A distinction is drawn between piloted missions (with a human pilot in the vehicle) and autonomous missions. If the mission is piloted, a fixed number of pilots per aircraft is used. If the mission is flown autonomously, the pilot cost model uses "bunker pilots": pilots who remain in a control center on the ground, ready to provide assistance remotely if needed [16]. A single bunker pilot is responsible for multiple aircraft, and so a fixed number of aircraft per bunker pilot is used. The same wrap rate is used in either case, regardless of whether the mission is piloted or autonomous. This approach is shown in Eqs. (6) and (7), respectively.

$$\text{Pilot cost} = \text{Pilot wrap rate} \times \text{Pilots per aircraft} \times \text{Mission time} \quad \text{(Piloted mission)} \tag{6}$$

$$= \frac{\text{Pilot wrap rate} \times \text{Mission time}}{\text{Aircraft per bunker pilot}} \quad \text{(Autonomous mission)} \tag{7}$$

Maintenance costs are estimated using a fixed number of maintenance man-hours per flight hour, together with a mechanic wrap rate, and 0.25–1 maintenance man-hours per flight hour are typical for light aircraft [13]; wrap rates of $53–$67 per hour are typical for general-aviation mechanics [15].

Energy cost is computed by multiplying the amount of electricity used during the mission by the price of electricity: $0.12 per kWh, the average price of electricity in the United States [16]. Finally, IOC is estimated as a fixed fraction of DOC. Values of 33–100% are typical for airlines, depending on the business model [13]. A value of 40% is used in this work.

3. *Trip Cost*

A distinction is made between trip cost and mission cost. Mission cost is simply the sum of capital expenses (amortized) and operating expenses for a given mission. Mission costs are therefore computed separately for the revenue and deadhead missions. Trip cost is then computed using Eq. (8):

$$\text{Cost per trip} = (1 + \text{margin})[(\text{Cost per revenue mission}) + \frac{dr}{1 - dr}(\text{Cost per deadhead mission})] \tag{8}$$

dr is the deadhead ratio: number of deadhead missions as a percentage of total number of missions. A deadhead ratio of 35% is used in this work; the cost margin is set to 10%.

Cost per passenger kilometer is obtained by normalizing the trip cost using the range and number of passengers from the revenue mission. Deadhead effect and cost margin are thus both included.

4. *Limitations*

A number of important effects are not included in the cost model. For example, the same airframe purchase price per unit empty mass is used for all configurations. This may not be an accurate assumption. For example, the lift + cruise configuration is aeromechanically quite simple as compared with configurations with more moving parts like the tilt wing and tilt rotor. It should therefore benefit from lower development, certification, and manufacturing costs, resulting in a reduced purchase price. Several other costs are not modeled, including taxes, insurance, landing fees, air traffic control fees, and profit margin. The aforementioned 10% cost margin is included to account for these effects.

However, it turns out that the cost model does not directly affect vehicle sizing. If only the vehicle and sizing-mission models are considered and maximum takeoff weight is used as the objective function, the optimizer returns exactly the same vehicle and performance data as if the revenue mission, deadhead mission, and cost model are included and cost per trip is the objective. Therefore, the cost model can be regarded as a first-order analysis, using data from a vehicle that is optimized for the sizing mission.

III. Results

A. Configurational Trade Study

1. *Inputs*

Configuration-specific input data are given in Table 7. An example for each configuration is listed; values for number of rotors N were taken from their respective examples. Cruising speed values were taken from Ref. [3]. Reference [3] also gives a range of values for cruise lift-to-drag ratio and hover disk loading; the median values are used in this study. Loiter speed and lift-to-drag ratio values are estimated from the cruise values, using the method in Appendix A.

As discussed in Sec. II.B.1, a constant empty mass fraction is assumed for each configuration. A recent eVTOL study by Duffy et al. [17] used configuration-specific structural, propulsion-system, and fixed-equipment mass models. Three eVTOL configurations were evaluated: a helicopter, a stopped rotor (lift + cruise), and a tilt rotor. Empty mass fractions of 0.43, 0.53, and 0.55 were, respectively, obtained, and used to estimate the values in Table 7.

Table 7 Input data for each configuration

				Cruise		Hover	
Configuration	Example	f_e	N	V, m/s	L/D	$(T/A)_{\max}$, N/m^2	$(\overline{C_l})_{\max}$
Lift + cruise	Aurora PAV	0.53	8	67	10	718	1.0
Compound heli	Airbus X^3	0.5	1	67	9	215	0.8
Tilt wing	A^3 Vahana	0.55	8	67	12	718	1.0
Tilt rotor	Joby S2	0.55	12	67	14	718	1.0
Helicopter	Robinson R44	0.43	1	45	4.25	215	0.6
Coaxial heli	Kamov Ka-32	0.43	2	67	5.5	335	0.6
Multirotor	Ehang 184	0.43	8	22	1.5	180	0.6
Autogyro	Magni M24	0.5	1	45	3.5	180	0.8
Tilt duct	Lilium Jet	0.55	36	67	10	1915	1.0

Note that not all of the examples represent eVTOL concepts.

As discussed in Sec. II.B.3, rotor tip speed is a design variable. The optimizer tends to reduce the tip speed as much as possible, to reduce blade profile drag losses. Therefore, the tip speed is effectively set by its lower limit: a constraint on blade mean lift coefficient.

Helicopters typically operate with $\overline{C_l}$ between 0.3 and 0.6 [8]. This is because helicopters with higher values of $\overline{C_l}$ would be prone to retreating blade stall in forward flight. For this reason, $\overline{C_l}$ is constrained to below 0.6 for the conventional and coaxial helicopter.

Retreating blade stall is only an issue for configurations that use their rotors to provide lift in cruise. Therefore, configurations like the tilt rotor and lift + cruise, which do not use their rotors to provide lift in cruise, use a $\overline{C_l}$ constraint of 1.0. In theory, values as high as 1.5–1.6 could be used before the rotor stalls; the value of 1.0 provides a margin for control in hover. The compound helicopter uses its rotor to provide some (but not all) lift in cruise; a $\overline{C_l}$ constraint of 0.8 is used. The same value is used for the autogyro.

Although Table 7 includes parameter estimates for the autogyro and the tilt duct, they are not included in the results. This is because the vehicle performance model does not accurately describe these two configurations. For example, all three mission profiles include hover segments, but an autogyro is incapable of hover. Instead, the main rotor is unpowered, and autorotates in flight. Meanwhile, the tilt duct uses multiple ducted fans to provide lift in hover. These ducts provide an efficiency and noise benefit, relative to an unducted rotor [13]. In the absence of a model for taking these two benefits into account, the tilt duct is neglected.

Conventional and compound helicopters both have tail rotors, which consume additional power in cruise and in hover. This is accounted for using the method in Appendix B.

2. *Results*

A bar chart with some key results from the configurational trade study is shown in Fig. 2. Additional results are given in Table 8. Note that all times are from the revenue mission; rotor performance data are from the sizing mission.

The multirotor, conventional helicopter, and coaxial helicopter are all missing from Fig. 2. In the case of the multirotor, the optimizer returns primal infeasible; i.e., a solution for this configuration that satisfies all of the requirements and constraints does not exist.[‡‡] The conventional and coaxial helicopters do return a feasible solution, but at significantly higher takeoff masses: above 4500 kg and above 2700 kg, respectively. Costs are also significantly higher. They were therefore dropped from consideration.

The four remaining configurations are the lift + cruise aircraft, the compound helicopter, the tilt wing, and the tilt rotor. These configurations all have a relatively high lift-to-drag ratio, but also (with the exception of the compound helicopter) a relatively high disk loading. Because a high lift-to-drag ratio translates to increased efficiency in cruise, whereas a low disk loading translates to increased efficiency in hover, this means that cruise efficiency takes precedence over hover efficiency for the mission under consideration.

Figure 2b shows that significant amounts of energy are consumed during all three categories of mission segment (cruise, hover, and reserve). Figure 2c shows that reserve power is lower than cruise power, due to the loiter adjustments discussed in Appendix A. Also, all four aircraft consume significantly more power in hover than in cruise. The compound helicopter has the highest power draw in cruise, due to its low lift-to-drag ratio; it also has the lowest power draw in hover, due to its low disk loading. This configuration has the highest trip cost, further supporting the conclusion that cruise efficiency takes precedence over hover efficiency.

Flight times from Fig. 2d for all four configurations are identical, because they all have the same hover time and cruising speed (Tables 4 and 7, respectively). However, configurations that use more energy take longer to charge, and so the corresponding mission times are greater. Furthermore, charging the battery takes almost as long as flying the mission in some cases. To increase the number of missions that can be conducted during a given time period (e.g., during rush hour), more powerful battery chargers are required.

Costs vary somewhat between configurations. Figure 2e shows that cost per passenger kilometer (including deadhead effects) ranges from as low as \$2.37 for the tilt rotor to about \$3.20 for the compound helicopter. For comparison, the average prices of UberX and UberPool[§§] rides in the United States in September 2016 were \$1.45 per passenger kilometer (\$2.34 per passenger mile) and \$0.86 per passenger kilometer (\$1.38 per passenger mile), respectively [16]. Note that any direct cost comparison must be carefully qualified, due to the cost model limitations discussed in Sec. II.D.4.

Figure 2f shows that the portion of trip cost attributable to the deadhead mission is not very large, as compared with that attributable to the revenue mission. This is partly because of the low deadhead ratio (Table 5); it is also because the deadhead mission is flown autonomously, with correspondingly lower pilot costs. Figures 2h and 2i show that operating expenses account for a somewhat larger share of revenue mission cost than capital expenses.

Figure 2g shows that a relatively small share of the purchase price is attributable to the battery. However, Fig. 2h shows that the battery accounts for a much larger share (about two-thirds) of amortized mission capital expenses. This apparent contradiction is resolved by comparing the amortization methods. Recall from Sec. II.D.1 that the airframe and avionics are amortized using a 10,000 h service life, whereas the battery is amortized using an 800-cycle life (i.e., 800 missions). Meanwhile, Fig. 2i shows that pilot cost dominates operating expenses. Therefore, the keys to reducing the cost per trip are to 1) reduce battery manufacturing cost, 2) increase battery cycle life (both of which reduce battery amortized costs), and 3) implement vehicle autonomy (which lowers pilot cost).

[‡‡]Recall from Sec. II.A that geometric programs are guaranteed to return a globally optimal solution, if one exists.

[§§]UberX is the standard car ride-sharing option, where the ride is paid for by one passenger. UberPool involves splitting the ride between multiple paying passengers, all with different origins and/or destinations. It generally costs less than UberX, but trips take longer to complete.

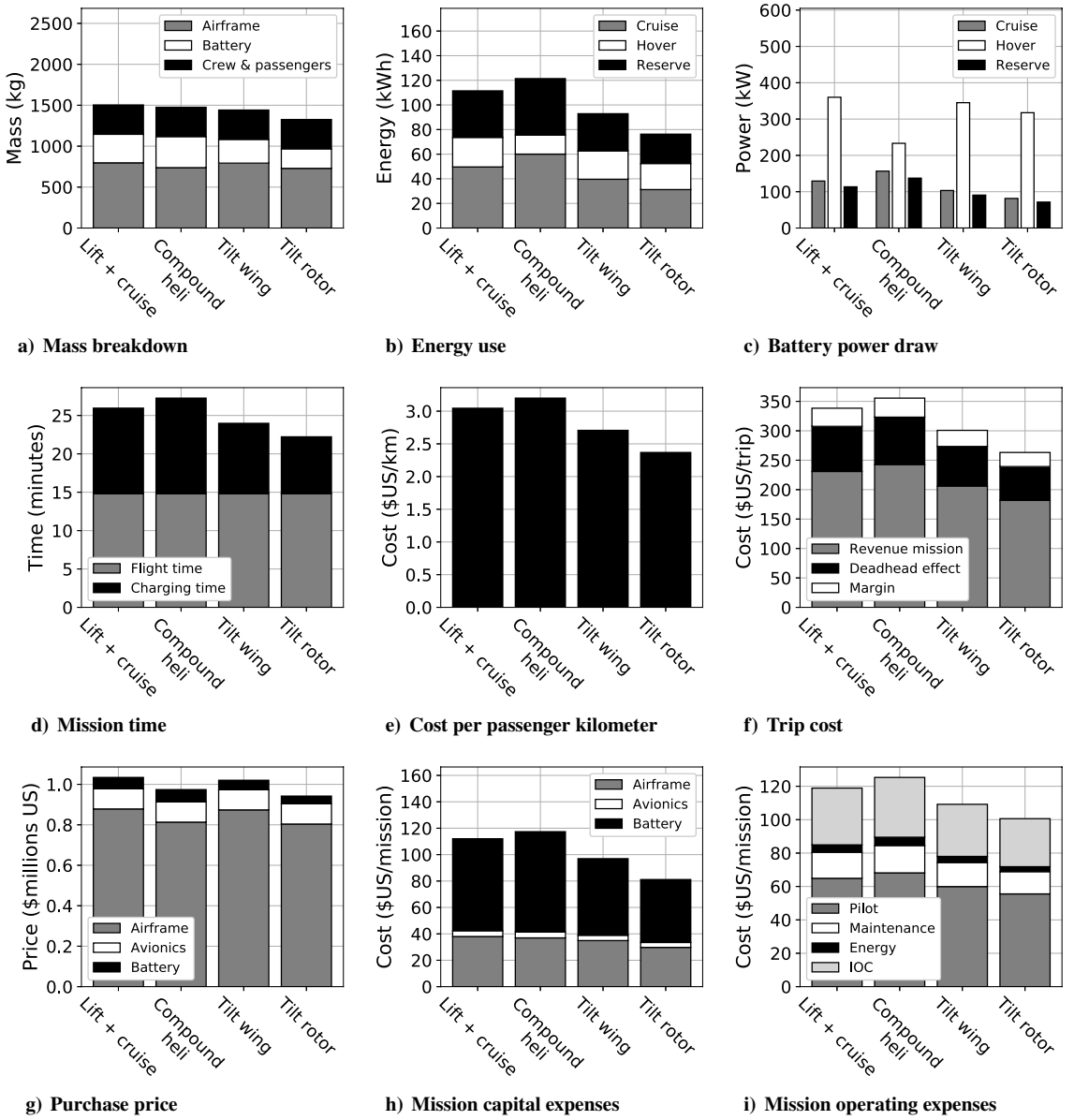

a) Mass breakdown b) Energy use c) Battery power draw

d) Mission time e) Cost per passenger kilometer f) Trip cost

g) Purchase price h) Mission capital expenses i) Mission operating expenses

Fig. 2 Results from the configurational trade study. Capital and operating expense breakdowns are from the revenue mission.

Table 8 Additional results from the configurational trade study

Configuration	Lift + cruise	Compound heli	Tilt wing	Tilt rotor	Unit
Maximum takeoff mass	1504	1475	1441	1326	kg
Airframe mass	797	738	793	729	kg
Battery mass	348	379	290	238	kg
Mission time	26.0	27.3	24.0	22.2	min
Flight time	14.8	14.8	14.8	14.8	min
Charging time	11.1	12.5	9.2	7.4	min
Purchase price	1.034	0.974	1.020	0.942	$US (millions)
Trip cost	338	356	301	263	$US
Cost per passenger-km	3.04	3.20	2.71	2.37	$US
Rotor diameter	1.81	9.25	1.77	1.39	m
Tip speed	187.6	114.9	187.6	187.6	m/s
Tip Mach number	0.55	0.34	0.55	0.55	— —
Thrust coefficient	0.0333	0.0267	0.0333	0.0333	— —
Power coefficient	0.0039	0.0029	0.0039	0.0039	— —
Figure of merit	0.78	0.76	0.78	0.78	— —

Purchase prices include all components (airframe, avionics, and battery).

B. Case Study: New York City Airport Transfers

New York City was selected as an example city in which to implement a UAM service. Air taxi services already exist in the city, provided by companies such as Blade[¶¶] and New York Helicopter.[***] New York Helicopter provides airport transfer services between downtown heliports and local airports. Three downtown heliports are listed on their website: East 34th Street, West 30th Street, and Pier 6. Transfers are provided to three airports: John F. Kennedy (JFK), LaGuardia (LGA), and Newark (EWR). Uber recently introduced a similar service, which they call Uber Copter [18].

The flight distance between each heliport and each airport was computed using Google Maps. Two options are available: a direct route and an overwater-only route. As-the-crow-flies routes are generally not permitted in New York City. Instead, the city has defined routes that helicopters must follow. The direct route was selected as the shortest of the existing helicopter routes. Overwater-only flights are included as an option to reduce community noise exposure.

Computed flight distances are presented in Table 9. Note that in some cases, no direct route exists that is shorter than the overwater route. In these cases, direct and overwater route distances are identical.

The longest direct and overwater routes in Table 9 are West 30th Street to JFK (30.3 km; 16.3 nmi) and East 34th Street to JFK (47.7 km; 25.7 nmi), respectively. They are shown in Fig. 3.

Based on Table 9, trip distances of 35 km (19 nmi) for the direct flight and 56 km (30 nmi) for the overwater flight were selected. A comparative study was conducted, using three sets of mission inputs:

1) A 35 km sizing mission and a 35 km revenue mission: This vehicle is solely capable of flying the direct route.

2) A 56 km sizing mission and a 35 km revenue mission: This vehicle flies the direct route when carrying passengers, but has the range to fly the overwater route if necessary.

3) A 56 km sizing mission and a 56 km revenue mission: This vehicle always flies the overwater route.

The revenue and deadhead mission ranges are identical. Results are in Fig. 4.

Figure 4a shows that vehicle mass is not strongly affected by the mission selection. In particular, there is no difference between options 2 and 3. However, Fig. 4c shows that the effect on trip cost is significant. Flying a direct route results in substantial cost savings, even if the vehicle is sized to fly the overwater mission; this is mainly due to the reduced pilot and maintenance costs. Flight time is independent of configuration, for reasons discussed in Sec. III.A.2.

Figure 4c shows that costs for a two-passenger trip range from \$170 to \$280 (\$85 to \$140 per passenger), depending on configuration and mission. For comparison, New York Helicopter quotes a price of \$1900 per airport transfer (i.e., \$950 per passenger for a two-passenger trip) on their website. Uber estimates that their service costs \$200–\$225 per passenger (i.e., \$400–\$450 for a two-passenger trip), whereas Blade announced that its service costs only \$195 per passenger (\$390 for a two-passenger trip) [18]. Recall again the cost model limitations discussed in Sec. II.D.4; a comparison of cost numbers must be qualified appropriately. However, the analysis presented here shows that a UAM service is, at worst, comparable to existing helicopter services in terms of cost.

A UAM service would also have to compete with existing car ride-sharing services. Time and price data for rides to JFK are presented in Table 10. Data were gathered using the Uber smartphone application, between 4:00 p.m. and 4:10 p.m. EST on Thursday, August 15, 2019 (i.e., during rush hour). Note that the Uber app gives a range of trip times (rather than one value) if UberPool is selected.

Table 10 shows that a UAM service may cost more relative to car ride-sharing, but is superior in terms of trip time. Cost per trip values from Fig. 4 (\$170–\$280) are somewhat higher than those for UberPool, UberX, and UberBlack rides, and are comparable to those for UberBlack SUV rides.[†††] However, Fig. 4b shows that UAM mission times are much shorter: 15–25 min, of which only 10–15 min is flight time. By contrast, a ride-sharing trip requires at least 59–85 min, depending on the heliport of origin.

Table 9 Flight distance for the airport transfer routes

		Distance, km	
Heliport	Airport	Direct	Overwater
West 30th Street	JFK	30.3	45.2
	LGA	26.2	26.2
	EWR	24.7	24.7
East 34th Street	JFK	18.3	47.7
	LGA	11.8	11.8
	EWR	26.5	26.5
Pier 6	JFK	19.2	40.2
	LGA	18.4	18.4
	EWR	19.6	19.6

This trip time benefit can be analyzed using a value of travel time savings (VTTS) approach. VTTS values are given by the U.S. Department of Transportation (DOT) [19]. Airport transfers are assumed to form part of intercity trips, and so the intercity VTTS values are used. Three trip purposes are represented: personal, business, and all purposes (average of the two, weighted by number of person-trips). The values given by Ref. [19] are based on 2015 median household income; they are adjusted to 2018 (the latest year for which median household income data from the U.S. Census Bureau is available). Resulting values are listed in Table 11.

A "VTTS penalty" is then defined, based on the difference between the trip time via car ride-sharing and that via air taxi:

$$\text{VTTSpenalty} = \text{VTTS} \times [t_{\text{rideshare}} - (t_{\text{flight}} + t_{\text{ground}} + t_{\text{boarding}})] \quad (9)$$

$t_{\text{rideshare}}$ is the time required for a car ride-sharing trip. The time required to travel via air taxi is the sum of the flight time, ground time (time required to travel to the heliport), and boarding time: t_{flight}, t_{ground}, and t_{boarding}, respectively. t_{flight} is obtained from Fig. 4b, assuming an overwater revenue mission; t_{ground} is set to 15 min; and t_{boarding} is set to 5 min (see Sec. II.C). Because a range of values for UberPool trip time are given in Table 10, $t_{\text{rideshare}}$ is set equal to the median.

Ride-sharing trip prices from Table 10, along with VTTS penalties, are plotted in Fig. 5.

Figure 5 shows that prices and penalties vary depending on heliport of origin, ride option, and trip purpose. VTTS penalties are highest for business trips, because their VTTS values are larger. East 34th Street has the shortest ride-sharing trip times to JFK; as a consequence, prices and VTTS penalties are lower than for the other two heliports. VTTS penalties for UberPool trips are larger than those of the other ride options, because these trips take longer.

With VTTS penalties included, Fig. 5 shows that prices vary from \$100 to \$300. This is comparable to the aforementioned costs for a two-passenger trip via air taxi: \$170–\$280. Therefore, with VTTS effects included, a UAM service may be comparable to existing car ride-sharing services on cost.

New York City would be a difficult place to roll out a UAM service, because the primary restrictions on market size are particularly acute there. Vascik et al. [20] identified three primary constraints on UAM market size: availability of ground infrastructure, interaction with air traffic control, and community acceptance of aircraft noise. New York City has some of the highest real-estate prices in the world, so obtaining space for additional heliports, charging stations, and maintenance facilities would be very expensive; with three large international airports and numerous smaller ones in the area, the airspace ranks among the world's busiest (second only to London); and community opposition to noise is already a major issue for the city's helicopter tour operators [21]. UAM operators must take these factors into account.

[¶¶]BLADE—The Sharpest Way to Fly: https://www.flyblade.com/ [retrieved 30 October 2017].

[***]New York City Helicopter Tours: https://www.newyorkhelicopter.com/ [retrieved 30 October 2017].

[†††]UberBlack and UberBlack SUV differ from UberX and UberPool in that luxury cars and professional drivers are employed.

a) The longest direct route: West 30th Street to JFK

b) The longest overwater route: East 34th Street to JFK

Fig. 3 New York City helicopter routes (black lines). Note that the direct route passes over Brooklyn.

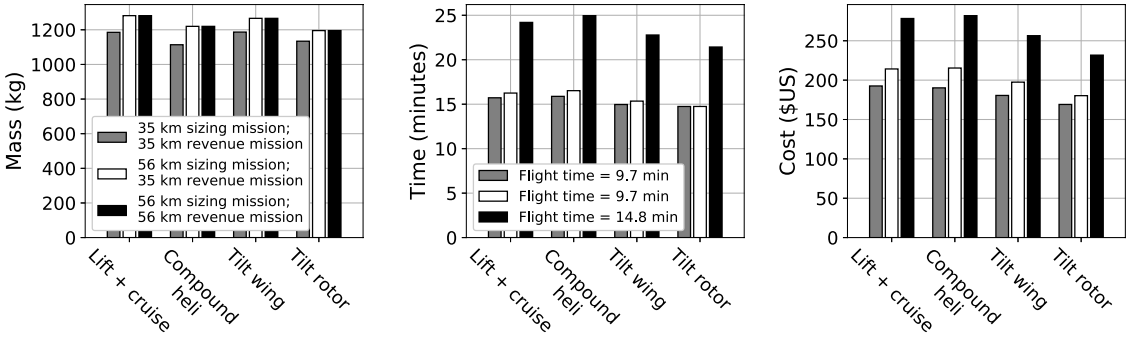

a) Maximum takeoff mass b) Mission time c) Trip cost

Fig. 4 Results from the New York City case study.

Table 10 Time and cost data by heliport of origin, for car ride-sharing trips to JFK

Heliport	Ride option	Trip time, min	Price, $
West 30th Street	UberPool	86–111	69
	UberX	85	93
	UberBlack	85	142
	UberBlack SUV	87	204
East 34th Street	UberPool	80–104	68
	UberX	59	84
	UberBlack	59	129
	UberBlack SUV	62	186
Pier 6	UberPool	84–109	84
	UberX	79	108
	UberBlack	80	170
	UberBlack SUV	80	246

Table 11 VTTS values for intercity travel in 2018

Trip purpose	VTTS ($ per person-hour)
Personal	38.08
Business	66.66
All purposes	49.68

C. Sensitivity Analysis

1. Reserve Requirement

eVTOL developers are faced with a choice: should they certify their vehicles as airplanes or as helicopters? The FAA definitions are as follows [9]: "[airplane] means [a] fixed-wing aircraft ... that is supported in flight by the dynamic reaction of the air against its wings," whereas "[helicopter] means [an] aircraft that depends principally for its support in flight on the lift generated by one or more rotors." For configurations with wings as well as rotors, either definition applies, and so a choice must be made.

From a certification perspective, the most important difference is in the reserve requirement. Three reserve options are available. The first is the default used in this work: a 20-min loiter time, required by the FAA for helicopter VFR operations (see Sec. II.C). It would be applicable if eVTOL vehicles are certified as helicopters. The second reserve option is a 30-min loiter time, required by the FAA for aircraft VFR operations during the day [13]. This requirement would be applicable if eVTOL vehicles are certified as aircraft. The final option is a 3.7 km (2 nmi) diversion distance, included in case a special regulatory class is created for eVTOL aircraft. The General Aviation Manufacturer's Association (GAMA) is considering such an option for eVTOL aircraft certification, in part because (unlike a fixed-wing aircraft) an eVTOL is capable of landing in almost any open area in an emergency [22].

Each vehicle configuration was optimized for each reserve requirement option. All other parameter inputs are identical to

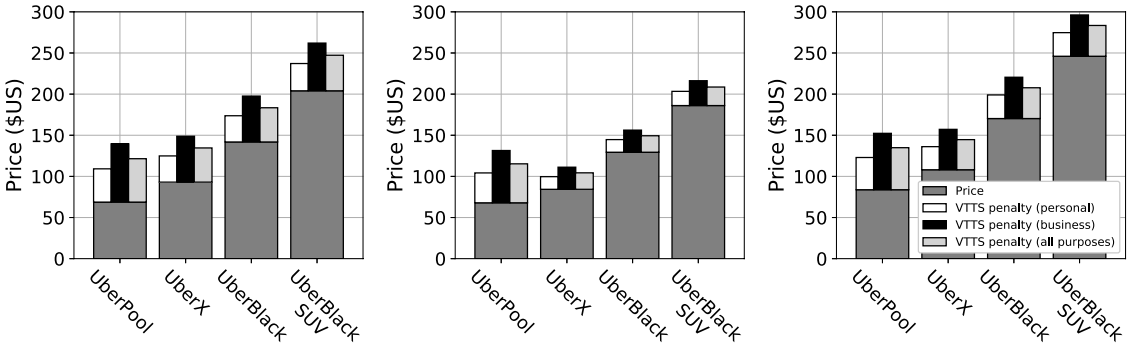

a) West 30th Street b) East 34th Street c) Pier 6

Fig. 5 Uber prices, including VTTS penalties.

those from the configurational trade study (Sec. III.A). Results are in Fig. 6.

Figures 6a and 6c show that vehicle mass and cost are strongly affected by the reserve requirement. This is particularly true in the case of the compound helicopter, for which the cost nearly doubles if the reserve requirement is changed from a 2-nmi diversion to a 30-min loiter. The flight time is 14.8 min, regardless of configuration or reserve requirement; the effect on mission time in Fig. 6b is entirely due to increased charging time.

It seems as first glance that the logical choice is the helicopter requirement. This choice reduces regulatory uncertainty by taking advantage of an existing certification framework, while providing a mass and cost reduction relative to the airplane requirement. However, helicopter pilots are in short supply relative to aircraft pilots. In 2018, approximately 100,000 pilots held commercial (fixed-wing) ratings in the United States; an additional 162,000 pilots held airline ratings [23]. By contrast, only 15,000 pilots held rotorcraft ratings. Barring full vehicle autonomy (which would require a change in FAA regulations), a pilot shortage would seriously impair the widespread adoption of UAM. Therefore, unless the regulations are changed, the choice of certification pathway should be carefully considered.

2. *Mission Range*

The sensitivity to the mission range requirement was estimated by varying the mission range, and optimizing each vehicle configuration accordingly. The same range requirement is used for the sizing, revenue, and deadhead missions; all other parameter inputs are held constant. Results are in Fig. 7.

Figure 7 shows that some configurations are more sensitive to mission range than others, especially at longer ranges (above about 100 km). The defining input parameter is cruise lift-to-drag ratio. The compound helicopter ($L/D = 9$, the lowest value) weighs and costs the most at longer ranges, whereas the tilt rotor ($L/D = 14$, the highest value) weighs and costs the least. Cost per passenger kilometer is minimized at a mission range of 50–100 km, depending on configuration. UAM is at its most cost-competitive (relative to other modes of transport) at this range; it may therefore be wise to use a range between 50 and 100 km as a design requirement.

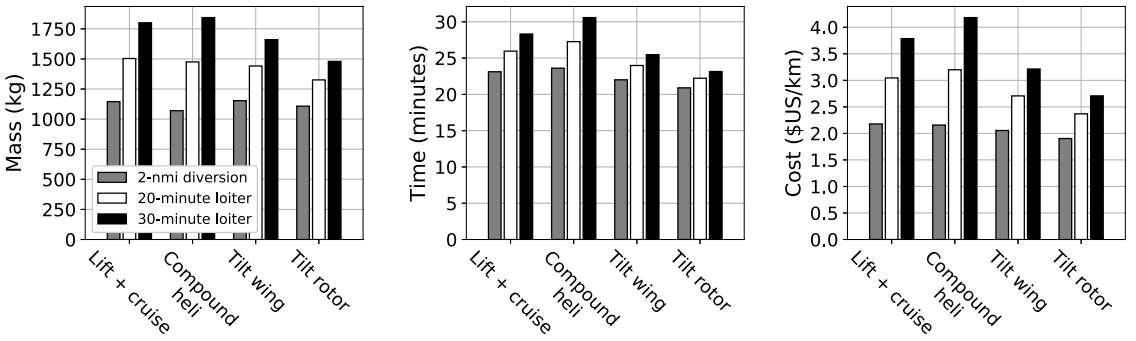

a) Maximum takeoff mass b) Mission time c) Cost per passenger kilometer

Fig. 6 Sensitivity to reserve requirement.

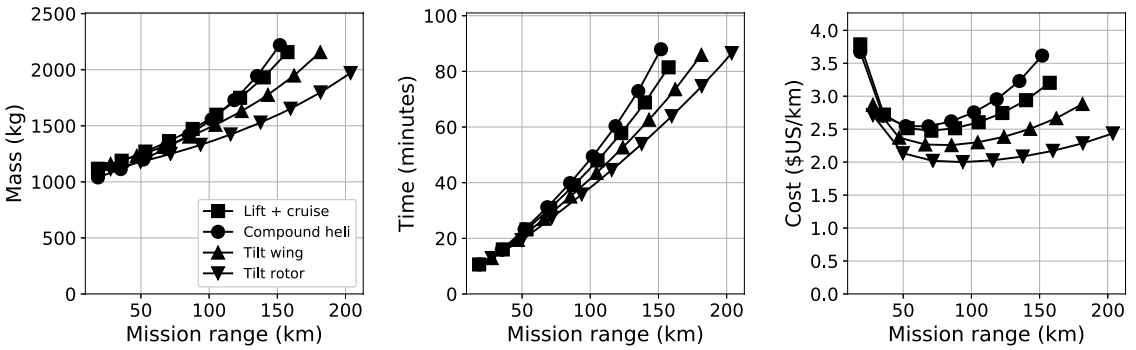

a) Maximum takeoff mass b) Mission time c) Cost per passenger kilometer

Fig. 7 Sensitivity to mission range.

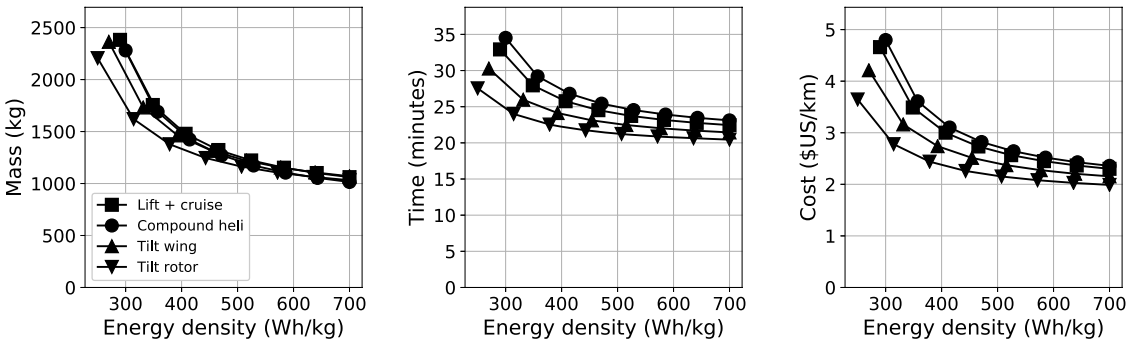

a) Maximum takeoff mass b) Mission time c) Cost per passenger kilometer

Fig. 8 Sensitivity to battery energy density.

3. Battery Energy Density

This study uses a battery pack energy density of 400 Wh/kg, a value not representative of current (commercially available) battery technology. For comparison, current lithium-ion battery cells are capable of only about 230–250 Wh/kg, not including pack-level effects [24]. Alternate battery chemistries such as lithium–sulfur may be capable of cell energy densities as high as 400–600 Wh/kg [25]. However, a number of issues with lithium–sulfur (e.g., safety, electrode stability, and cycle life) remain unsolved [25,26]. Whether such batteries will be commercially available by the time UAM services begin is uncertain.

The sensitivity to battery energy density was estimated by varying the energy density, and optimizing each vehicle configuration accordingly. Results are in Fig. 7.

Figure 8 shows that all four configurations are quite sensitive to battery energy density below around 400 Wh/kg, but less so above this point. Similar results have been obtained from other studies on electric aircraft [17,27]. This does not imply that eVTOL vehicles are infeasible without 400 Wh/kg batteries. Rather, 400 Wh/kg was selected because it represents a critical enabling value: a technology threshold above which energy density is no longer as significant a concern. Once the technology threshold is reached, eVTOL battery developers should instead focus on improving other battery parameters such as manufacturing cost and cycle life, due to their strong influence on trip cost (see Sec. III.A.2).

IV. Conclusions

A conceptual design and optimization tool for UAM was developed, using geometric programming. This tool was used to conduct a study of UAM from a vehicle design perspective. Trip cost, including the additional cost due to deadhead missions, was used as the objective function. For the selected mission, only four configurations are viable: the lift + cruise configuration, the compound helicopter, the tilt wing, and the tilt rotor. Configurations with a higher lift-to-drag ratio generally weigh and cost less to operate, despite their higher hover disk loading. The two most important costs are pilot salary and battery amortized cost. The keys to lowering the price of a UAM service are therefore to implement vehicle autonomy, reduce battery manufacturing costs, and increase battery cycle life.

The New York City case study showed that a UAM service may provide a trip cost advantage relative to current helicopter air taxi operations. UAM would provide a trip time benefit relative to current car ride-sharing operations, but would probably cost more. If this tradeoff is modeled using estimated VTTS, then a UAM service may be comparable to existing car ride-sharing services in terms of cost. Furthermore, vehicle design may be impacted by requirements specific to a given city. In the case of New York City, an overwater-only flight restriction, imposed for community noise reasons, would adversely affect costs and cannot be ignored by vehicle designers.

Sensitivity analysis reveals that the choice of reserve requirement is critical. Pilot availability, certification risk, vehicle mass, and trip cost must all be carefully balanced. Meanwhile, cost per passenger kilometer is minimized for missions range requirements between 50 and 100 km. UAM is at its most cost-competitive at this range. Finally, a battery energy density of 400 Wh/kg is a critical enabling value for UAM.

Appendix A: Loiter Model Adjustments

Cruising speed and cruise lift-to-drag ratio for each configuration are given in Table 7. These numbers are used in cruise, and also for the reserve segment if a 2-nmi diversion requirement is used (as in Sec. III.C.1). However, the FAA reserve requirement is a loiter requirement, as opposed to a cruise requirement. For this reason, the optimal lift-to-drag ratio and flight speed during the reserve segment differ from the cruise values.

If a parabolic drag polar is assumed, Eqs. (4) and (5) can be written as Eqs. (A1) and (A2), respectively:

$$\text{Range} = \eta \frac{C_L}{C_{D_0} + kC_L^2} \frac{E_b}{W} \tag{A1}$$

$$\text{Endurance} = \eta \left[\frac{\rho S C_L}{2\ \text{W}}\right]^{1/2} \frac{C_L}{C_{D_0} + kC_L^2} \frac{E_b}{W} \tag{A2}$$

C_L is the wing three-dimensional lift coefficient, C_{D_0} is the aircraft three-dimensional zero-lift drag coefficient, and k is the aircraft induced power factor. All values are referenced to the wing area S. k is equal to $1/(\pi eAR)$, where e is the span efficiency and AR is the wing aspect ratio. ρ is the air density.

The conditions for maximum range and endurance can be obtained by differentiating Eqs. (A1) and (A2), respectively, with respect to lift coefficient. Algebraic manipulation then yields the optimal values for lift coefficient, airspeed, and lift-to-drag ratio, given in Table A1.

Therefore, if the cruising speed and lift-to-drag ratio for a given configuration are known, the loiter speed and lift-to-drag ratio can be estimated using Eqs. (A3) and (A4), respectively:

$$V_{\text{loiter}} = \left[\frac{1}{3}\right]^{1/4} V_{\text{cruise}} \tag{A3}$$

$$\left(\frac{L}{D}\right)_{\text{loiter}} = \frac{\sqrt{3}}{2}\left(\frac{L}{D}\right)_{\text{cruise}} \tag{A4}$$

Table A1 Flight conditions for maximum range and endurance

Condition	Max range	Max endurance
C_L	$\left[\frac{C_{D_0}}{k}\right]^{1/2}$	$\left[\frac{3C_{D_0}}{k}\right]^{1/2}$
V	$\left[\frac{2W}{\rho S}\right]^{1/2}\left[\frac{k}{C_{D_0}}\right]^{1/4}$	$\left[\frac{2\,W}{\rho S}\right]^{1/2}\left[\frac{k}{3C_{D_0}}\right]^{1/4}$
$\frac{L}{D}$	$\frac{1}{2}\left[\frac{1}{kC_{D_0}}\right]^{1/2}$	$\frac{1}{4}\left[\frac{3}{kC_{D_0}}\right]^{1/2}$

Table B1 Power increase percentages for configurations with a tail rotor

	Power increase, %	
Configuration	Hover	Cruise
Conventional heli	15	15
Compound heli	15	10

The net effect of Eqs. (A3) and (A4) is to reduce power consumption (and by extension, energy use) during the loiter segment. This in turn provides a benefit to battery sizing. These adjustments were implemented in the optimization tool.

Appendix B: Tail-Rotor Power Adjustments

Conventional and compound helicopters both have tail rotors, which consume additional power beyond that predicted by the unmodified cruise and hover models (Secs. III.C.2 and III.C.3, respectively). The tail rotor of a helicopter typically consumes 10–15% of the power consumed by the main rotor [8]. This adjustment can be applied to the conventional helicopter in both cruise and hover. However, the wing of a compound helicopter unloads the main rotor in cruise, causing it (and by extension, the tail rotor) to consume less power. As the wing and rotor power for the compound helicopter in cruise cannot be separated by the mission model, the additional power percentage applied to the compound helicopter was reduced.

Power increase percentages for both configurations are given in Table B1. These adjustments were implemented in the optimization tool.

Acknowledgments

This work was funded in part by the MIT Arthur Gelb graduate fellowship, and also by the AIAA William T. Piper, Sr. General Aviation Systems Graduate Award. The authors wish to thank all those who contributed their insights to this work. In particular, Peter Belobaba, Carl Dietrich, Michael Duffy, John Hansman, Michel Merluzeau, Diana Siegel, and Parker Vascik are acknowledged. The authors would also like to thank Edward "Ned" Burnell and Warren "Woody" Hoburg for developing and maintaining GPkit, the open-source software package for solving geometric programs that was used throughout this research. Finally, the authors would like to thank one of the anonymous reviewers for their comments on the value of travel time savings calculations.

References

[1] Moore, M. D., "Concept of Operations for Highly Autonomous Electric Zip Aviation," *14th AIAA Aviation Technology and Integration and Operations (ATIO) Conference*, AIAA Paper 2012-5472, Sept. 2012. https://doi.org/10.2514/6.2012-5472

[2] Brelje, B. J., and Martins, J. R., "Electric, Hybrid, and Turboelectric Fixed-Wing Aircraft: A Review of Concepts, Models, and Design Approaches," *Progress in Aerospace Sciences*, Vol. 104, Jan. 2019, pp. 1–19. https://doi.org/10.1016/j.paerosci.2018.06.004

[3] McDonald, R., and German, B., "eVTOL Stored Energy Overview," *Uber Elevate Summit*, Uber Elevate Summit 2017, Dallas, TX, April 2017, pp. 14–20.

[4] Hoburg, W., and Abbeel, P., "Geometric Programming for Aircraft Design Optimization," *AIAA Journal*, Vol. 52, No. 11, 2014, pp. 2414–2426. https://doi.org/10.2514/1.J052732

[5] Kirschen, P. G., and Hoburg, W. W., "The Power of Log Transformation: A Comparison of Geometric and Signomial Programming with General Nonlinear Programming Techniques for Aircraft Design Optimization," *2018 AIAA/ASCE/AHS/ASC Structures, Structural Dynamics, and Materials Conference*, AIAA Paper 2018-0655, Jan. 2018. https://doi.org/10.2514/6.2018-0655

[6] Burton, M. J., and Hoburg, W. W., "Solar and Gas Powered Long-Endurance Unmanned Aircraft Sizing via Geometric Programming," *Journal of Aircraft*, Vol. 55, No. 1, 2018, pp. 212–225. https://doi.org/10.2514/1.C034405

[7] Courtin, C., Burton, M., Butler, P., Yu, A., Vascik, P., and Hansman, J., "Feasibility Study of Short Takeoff and Landing Urban Air Mobility Vehicles Using Geometric Programming," *2018 Aviation Technology, Integration, and Operations Conference*, AIAA Paper 2018-4151, June 2018. https://doi.org/10.2514/6.2018-4151

[8] Seddon, J., and Newman, S., *Basic Helicopter Aerodynamics*, 3rd ed., Wiley, Hoboken, NJ, 2011, Chap. 2. https://doi.org/10.2514/4.868610

[9] "14 CFR 91.151—Fuel Requirements for Flight in VFR Conditions," Dept. of Transportation, Federal Aviation Administration, Washington, D.C., 2017, https://www.law.cornell.edu/cfr/text/14/91.151 [retrieved 14 Aug. 2019].

[10] Holland, M., "Supercharger V3—Shocking Power & Smart Strategy by Tesla (Charts!)," CleanTechnica, San Francisco, CA, March 2019, https://cleantechnica.com/2019/03/08/supercharger-v3-shocking-power-smart-strategy-by-tesla-charts/ [retrieved 14 Aug. 2019].

[11] Jackson, P., Jane's All the World's Aircraft: Development and Production, 2019–2020, IHS Markit, London, 2019, pp. 954–955.

[12] Cole, W., and Frazier, A. W., "Cost Projections for Utility-Scale Battery Storage," U.S. Dept. of Energy, National Renewable Energy Lab. TP-6A20-73222, Golden, CO, June 2019.

[13] Raymer, D. P., *Aircraft Design: A Conceptual Approach*, 5th ed., AIAA, Reston, VA, 2012, Chap. 18. https://doi.org/10.2514/4.869112

[14] Severson, K. A., Attia, P. M., Jin, N., Perkins, N., Jiang, B., Yang, Z., Chen, M. H., Aykol, M., Herring, P. K., Fraggedakis, D., Bazant, M. Z., Harris, S. J., Chueh, W. C., and Braatz, R. D., "Data-Driven Prediction of Battery Cycle Life Before Capacity Degradation," *Nature Energy*, Vol. 4, No. 5, 2019, pp. 383–391. https://doi.org/10.1038/s41560-019-0356-8

[15] Gudmundsson, S., *General Aviation Aircraft Design: Applied Methods and Procedures*, Butterworth-Heinemann, Oxford, 2013, Chap. 2.

[16] Holden, J., and Goel, N., "Fast-Forwarding to a Future of On-Demand Urban Air Transportation," Uber, Oct. 2016, pp. 41, 89–95, https://www.uber.com/elevate.pdf.

[17] Duffy, M. J., Wakayama, S. R., Hupp, R., Lacy, R., and Stauffer, M., "A Study in Reducing the Cost of Vertical Flight with Electric Propulsion," *17th AIAA Aviation Technology, Integration, and Operations Conference*, AIAA Paper 2017-3442, June 2017. https://doi.org/10.2514/6.2017-3442

[18] Vora, S., "Uber Copter to Offer Flights from Lower Manhattan to J.F.K.," *New York Times*, 2019, https://www.nytimes.com/2019/06/05/travel/uber-helicopter-nyc-jfk.html [retrieved 5 June 2019].

[19] White, V., "Revised Departmental Guidance on Valuation of Travel Time in Economic Analysis," U.S. Dept. of Transportation TM, Washington, D.C., Sept. 2016, https://www.transportation.gov/sites/dot.gov/files/docs/2016%20Revised%20Value%20of%20Travel%20Time%20Guidance.pdf.

[20] Vascik, P. D., Hansman, R. J., and Dunn, N. S., "Analysis of Urban Air Mobility Operational Constraints," *Journal of Air Transportation*, Vol. 26, No. 4, 2018, pp. 133–146. https://doi.org/10.2514/1.D0120

[21] Chaban, M. A., "Deal Restricts Tourist Helicopter Flights over New York," *New York Times*, 2016, https://www.nytimes.com/2016/02/01/nyregion/deal-restricts-tourist-helicopter-flights-over-new-york.html [retrieved 31 Jan. 2016].

[22] German, B., Daskilewicz, M., Hamilton, T. K., and Warren, M. M., "Cargo Delivery by Passenger eVTOL Aircraft: A Case Study in the San Francisco Bay Area," *2018 AIAA Aerospace Sciences Meeting*, AIAA Paper 2018-2006, Jan. 2018. https://doi.org/10.2514/6.2018-2006

[23] Barlett, A., "U.S. Civil Airmen Statistics," Federal Aviation Administration, Washington, D.C., 2018, https://www.faa.gov/data_research/aviation_data_statistics/civil_airmen_statistics/ [retrieved 16 Aug. 2019].

[24] Warwick, G., "Uber Pushing Hard for UAM," *Aviation Week and Space Technology*, Vol. 181, No. 16, Aug. 2018, pp. 38–40.

[25] Manthiram, A., Fu, Y., and Su, Y.-S., "Challenges and Prospects of Lithium-Sulfur Batteries," *Accounts of Chemical Research*, Vol. 46, No. 5, 2013, pp. 1125–1134. https://doi.org/10.1021/ar300179v

[26] Bruce, P. G., Freunberger, S. A., Hardwick, L. J., and Tarascon, J.-M., "Li-O_2 and Li-S Batteries with High Energy Storage," *Nature Materials*, Vol. 11, No. 1, 2012, pp. 19–29. https://doi.org/10.1038/nmat3191

[27] Patterson, M. D., German, B. J., and Moore, M. D., "Performance Analysis and Design of On-Demand Electric Aircraft Concepts," *AIAA Aviation Technology, Integration, and Operations (ATIO) Conference*, AIAA Paper 2012-5474, Sept. 2012. https://doi.org/10.2514/6.2012-5474